

Improved thermal property of strained InGaAlAs/AlGaAs quantum wells for 808-nm vertical cavity surface emitting lasers

Zhuang-Zhuang Zhao(赵壮壮), Meng Xun(荀孟), Guan-Zhong Pan(潘冠中), Yun Sun(孙昀), Jing-Tao Zhou(周静涛), and De-Xin Wu(吴德馨)

Citation: Chin. Phys. B, 2022, 31 (**3**): 034208. DOI: 10.1088/1674-1056/ac16d0
Journal homepage: http://cpb.iphy.ac.cn; http://iopscience.iop.org/cpb

What follows is a list of articles you may be interested in

Solar energy full-spectrum perfect absorption and efficient photo-thermal generation

Zhefu Liao(廖喆夫), Zhengqi Liu(刘正奇), Qizhao Wu(吴起兆), Xiaoshan Liu(刘晓山), Xuefeng Zhan(詹学峰), Gaorong Zeng(曾高荣), and Guiqiang Liu(刘桂强)

Chin. Phys. B, 2021, 30 (**8**): 084206. DOI: 10.1088/1674-1056/ac0696

An approach to gas sensors based on tunable diode laser incomplete saturated absorption spectra

Wei Nie(聂伟), Zhen-Yu Xu(许振宇), Rui-Feng Kan(阚瑞峰), Mei-Rong Dong(董美蓉), and Ji-Dong Lu(陆继东)

Chin. Phys. B, 2021, 30 (**6**): 064213. DOI: 10.1088/1674-1056/abd769

A pressure-calibration method of wavelength modulation spectroscopy in sealed microbial growth environment

Kun-Yang Wang(王坤阳), Jie Shao(邵杰), Li-Gang Shao(邵李刚), Jia-Jin Chen(陈家金), Gui-Shi Wang(王贵师), Kun Liu(刘琨), and Xiao-Ming Gao(高晓明)

Chin. Phys. B, 2021, 30 (**5**): 054203. DOI: 10.1088/1674-1056/abda32

Analysis of relative wavelength response characterization and its effects on scanned-WMS gas sensing

Dao Zheng(郑道), Zhi-Min Peng(彭志敏), Yan-Jun Ding(丁艳军), and Yan-Jun Du(杜艳君)

Chin. Phys. B, 2021, 30 (**4**): 044210. DOI: 10.1088/1674-1056/abdb1c

Research progress in terahertz quantum-cascade lasers and quantum-well photodetectors

Zhi-Yong Tan(谭智勇), Wen-Jian Wan(万文坚), Jun-Cheng Cao(曹俊诚)

Chin. Phys. B, 2020, 29 (**8**): 084212. DOI: 10.1088/1674-1056/aba945

Improved thermal property of strained InGaAlAs/AlGaAs quantum wells for 808-nm vertical cavity surface emitting lasers

Zhuang-Zhuang Zhao(赵壮壮), Meng Xun(荀孟)†, Guan-Zhong Pan(潘冠中), Yun Sun(孙昀), Jing-Tao Zhou(周静涛), and De-Xin Wu(吴德馨)

Institute of Microelectronics, Chinese Academy of Sciences, Beijing 100029, *China*

(Received 30 May 2021; revised manuscript received 4 July 2021; accepted manuscript online 22 July 2021)

The 808-nm vertical cavity surface emitting laser (VCSEL) with strained $In_{0.13}Ga_{0.75}Al_{0.12}As/Al_{0.3}Ga_{0.7}As$ quantum wells is designed and fabricated. Compared with the VCSELs with $Al_{0.05}Ga_{0.95}As/Al_{0.3}Ga_{0.7}As$ quantum wells, the VCSEL with strained $In_{0.13}Ga_{0.75}Al_{0.12}As/Al_{0.3}Ga_{0.7}As$ quantum wells is demonstrated to possess higher power conversion efficiency (PCE) and better temperature stability. The maximum PCE of 43.8% for 10-μm VCSEL is achieved at an ambient temperature of 30 °C. The size-dependent thermal characteristics are also analyzed by characterizing the spectral power and output power. It demonstrates that small oxide-aperture VCSELs are advantageous for temperature-stable performance.

Keywords: 808-nm VCSEL, InGaAlAs/AlGaAs quantum wells, thermal property

PACS: 42.55.Px, 42.55.Sa, 73.21.Fg **DOI:** 10.1088/1674-1056/ac16d0

1. Introduction

Vertical cavity surface emitting lasers (VCSELs) have significant advantages such as circular output beams, low threshold currents, single longitudinal modes, high speed modulations, slow wavelength shift rates *versus* temperature, and easy two-dimensional integrations.[1–6] The VCSELs have been widely used in data communication and short-distance optical interconnection.[7–11] In recent years, the VCSELs have been greatly developed and widely used in the fields of three-dimensional face recognition, hand gesture recognition, and laser radar.[12]

The wavelength of 808 nm is a very important wavelength in high-power laser applications. For example, the 808-nm laser source can be used as a pump source of solid-state laser (Nd:YAG or $Nd:YVO_4$) used for material cutting, marking, printing, *etc*.[13–15] The 808-nm pulsed laser sources are also used in the medical field for skin-care related cosmetic applications such as hair removal,[16] and they also used as industrial and military infra-red illumination sources.[17,18] Compared with the conventional 808-nm edge-emitting semiconductor lasers, VCSELs have good wavelength stability for varying environment temperatures. The VCSELs also exhibit a small divergence angle and circular output beam, which is conducive to the collimation or focusing.

To date, there have been not many reports on 808-nm VCSELs. These reports focused mainly on how to solve the heat dissipation problem in order to increase the output power in practical applications. Because of strong GaAs absorption at 808 nm, a bottom-emitting configuration cannot be used for efficient heat dissipations. Seurin *et al.* demonstrated 3 mm×3 mm arrays and 5 mm×5 mm arrays with the GaAs substrate completely removed from and mounted on diamond submounts. These arrays emit more than 50 W and 120 W, respectively, and exhibit a maximum power conversion efficiency of 42%.[19] Zhong *et al.* improved thermal stability of 808-nm VCSEL arrays by arranging the mesa distribution within the array in a nonlinear configuration.[20] Besides exploring heat dissipation measurement, it is also important to reduce the self-heating of the device for improving the temperature stability of the device. In VCSELs, the quantum well material is critical for differential gain and temperature stability. Zhang *et al.* numerically simulated $GaAs/Al_{0.3}Ga_{0.7}As$, $GaAs_xP_{1-x}/Al_{0.3}Ga_{0.7}As$ and $In_{1-x-y}Ga_xAl_yAs/Al_{0.3}Ga_{0.7}As$ quantum-well active regions. The output characteristics of the three designed quantum-well VCSELs were also calculated and compared.[21]

In this work, we design and fabricate two kinds of 808-nm VCSELs with $In_{0.13}Ga_{0.75}Al_{0.12}As/Al_{0.3}Ga_{0.7}As$ and $Al_{0.05}Ga_{0.95}As/Al_{0.3}Ga_{0.7}As$ quantum wells, respectively. The temperature characteristics of the two kinds of quantum wells are investigated mainly by theory. Then the output power characteristics and temperature characteristics of the fabricated VCSELs are analyzed in detail. The strained $In_{0.13}Ga_{0.75}Al_{0.12}As/Al_{0.3}Ga_{0.7}As$ quantum wells exhibit higher material gain and better temperature stability than $Al_{0.05}Ga_{0.95}As/Al_{0.3}Ga_{0.7}As$ quantum wells. The tested results are in good agreement with the calculations. The VCSELs with strained InAlGaAs quantum wells are more suitable for high temperature operation.

†Corresponding author. E-mail: xunmeng@ime.ac.cn

© 2022 Chinese Physical Society and IOP Publishing Ltd

2. Design and fabrication

The 808-nm top emitting laser layers to be examined here were grown by metal–organic chemical vapor deposition (MOCVD) on an N-type GaAs substrate. The bottom mirror consisted of 41.5 pairs of N-doped $Al_{0.25}Ga_{0.75}As/Al_{0.9}Ga_{0.1}As$ distributed Bragg reflectors (DBRs). The top mirror was composed of 23.5 pairs of P-doped $Al_{0.25}Ga_{0.75}As/Al_{0.9}Ga_{0.1}As$ DBRs. The active region contained three pairs of 6-nm-thick $In_{0.13}Ga_{0.75}Al_{0.12}As$ quantum wells surrounded by 8-nm-thick $Al_{0.3}Ga_{0.7}As$ barrier layers. Another kind of active region containing three pairs of 6-nm-thick $Al_{0.05}Ga_{0.95}As$ quantum wells surrounded by 8-nm-thick $Al_{0.3}Ga_{0.7}As$ barrier layers was also designed for contrast.

The fabrication procedure is as follows. Firstly, Ti/Pt/Au electrode was deposited at the periphery of output aperture. The P-DBRs were etched by inductively coupled plasma (ICP) reactive ion etching to expose the $Al_{0.98}Ga_{0.02}As$ layer. The oxide aperture was formed by the selective wet oxidation of $Al_{0.98}Ga_{0.02}As$ into Al_xO_y at temperature of 420 °C. A 200-nm-thick SiN layer was deposited on the surface of the VCSEL for electric isolation. After Ti/Au seed layer was sputtered, thick Au is electroplated to improve heat dissipation. Then, the substrate was thinned to 150 μm. The N-type electrode was evaporated on the substrate. Finally, the contacts are rapidly annealed in a nitrogen (N_2) ambient. Figure 1(a) shows a microscopic image of the fabricated 808-nm VCSELs. Figure 1(b) shows the cross-section diagram of the 808-nm VCSEL along the A–A′ direction in Fig. 1(a).

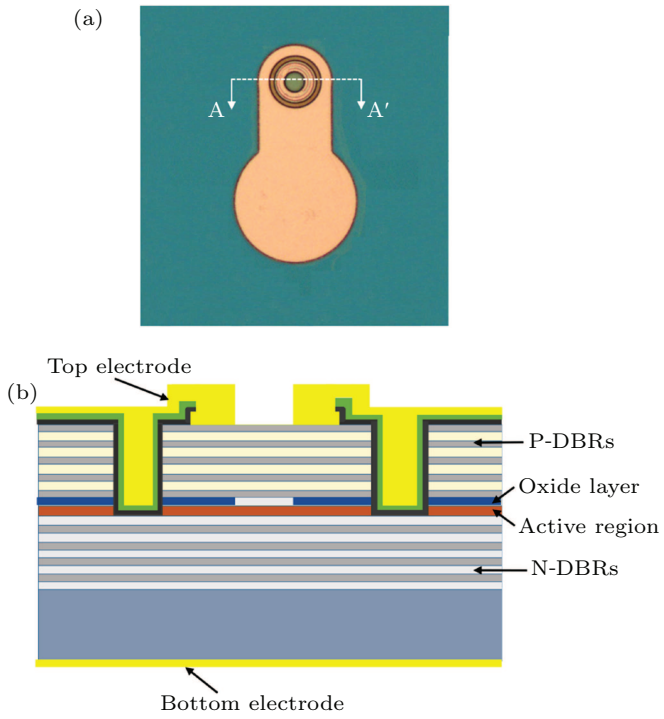


Fig. 1. (a) Microscopic image of actual device, and (b) cross-section diagram of device along A–A′ direction.

3. Results and discussion

The gains of $In_{0.13}Ga_{0.75}Al_{0.12}As/Al_{0.3}Ga_{0.7}As$ and $Al_{0.05}Ga_{0.95}As/Al_{0.3}Ga_{0.7}As$ quantum wells at different ambient temperatures are calculated by the standard 8-band $k \cdot p$ theory,[22] and the results are shown in Figs. 2(a) and 2(b). At the same ambient temperature, the gain of $In_{0.13}Ga_{0.75}Al_{0.12}As$ quantum wells is higher than that of $Al_{0.05}Ga_{0.95}As$ quantum wells. This is because the strain of $In_{0.13}Ga_{0.75}Al_{0.12}As$ quantum wells increases the curvature of the valence band structure, thereby greatly reducing the effective mass. The strain can reduce the valence band effective mass allowing the quasi-Fermi levels to separate more symmetrically. So not only does the material turns transparent faster, but also the gain increases faster with carrier density increasing.[23,24]

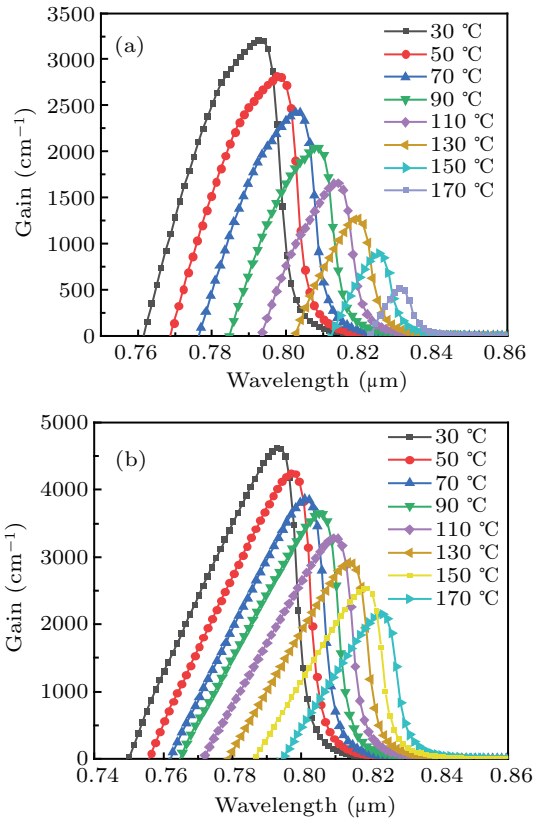


Fig. 2. (a) Curves of gain *versus* wavelength of three pairs of 6-nm-thick $In_{0.13}Ga_{0.75}Al_{0.12}As$ quantum wells surrounded by 8-nm-thick $Al_{0.3}Ga_{0.7}As$ barrier layers at different temperatures, and (b) curves of gain *versus* wavelength of three pairs of 6-nm-thick $Al_{0.05}Ga_{0.95}As$ quantum wells surrounded by 8-nm-thick $Al_{0.3}Ga_{0.7}As$ barrier layers at different temperatures.

Owing to increased leakage carriers at high temperatures, the gains of these two kinds of quantum wells decrease as the ambient temperature increases. The variation of the extracted peak gain with ambient temperature is shown in Fig. 3(a). The drop rate of $Al_{0.05}Ga_{0.95}As$ quantum wells' peak gain decreasing with ambient temperature increasing is 19.18 $cm^{-1}/°C$ which is faster than that of $In_{0.13}Ga_{0.75}Al_{0.12}As$ quantum wells, 17.26 $cm^{-1}/°C$. In addition, the gain curves of these two kinds of quantum wells are redshifted as the ambient

temperature increases. The red shift rate of the peak wavelength of $In_{0.13}Ga_{0.75}Al_{0.12}As$ quantum wells *versus* temperature increasing is 0.220 nm/°C which is slower than that of $Al_{0.05}Ga_{0.95}As$ quantum wells, 0.275 nm/°C as indicated in Fig. 3(b). The above calculation results show that the $In_{0.13}Ga_{0.75}Al_{0.12}As$ quantum wells exhibit higher material gain and better high-temperature stability than $Al_{0.05}Ga_{0.95}As$ quantum wells.

In addition, the gains of $Al_{0.05}Ga_{0.95}As$ and $In_{0.13}Ga_{0.75}Al_{0.12}As$ quantum wells with 4 nm and 8 nm in widths are also calculated at different ambient temperatures as shown in Fig. 4. The barrier material is still $Al_{0.3}Ga_{0.7}As$ with 8 nm in width. Obviously, the gains of the $In_{0.13}Ga_{0.75}Al_{0.12}As$ quantum wells with 4 nm and 8 nm in widths are significantly greater than those of the $Al_{0.05}Ga_{0.95}As$ quantum wells at the same ambient temperature. This trend agrees with the result of 6-nm quantum well in Fig. 2. From Figs. 2 and 4, the difference in gain between the two quantum wells turns smaller as the well width increases from 4 nm to 8 nm at the same temperature. As the well width is 4 nm, 6 nm, and 8 nm, the corresponding gain difference between the $In_{0.13}Ga_{0.75}Al_{0.12}As$ and $Al_{0.05}Ga_{0.95}As$ quantum wells is 2239.8 cm^{-1}, 1418.9 cm^{-1}, and 834.9 cm^{-1} at temperature of 30 °C.

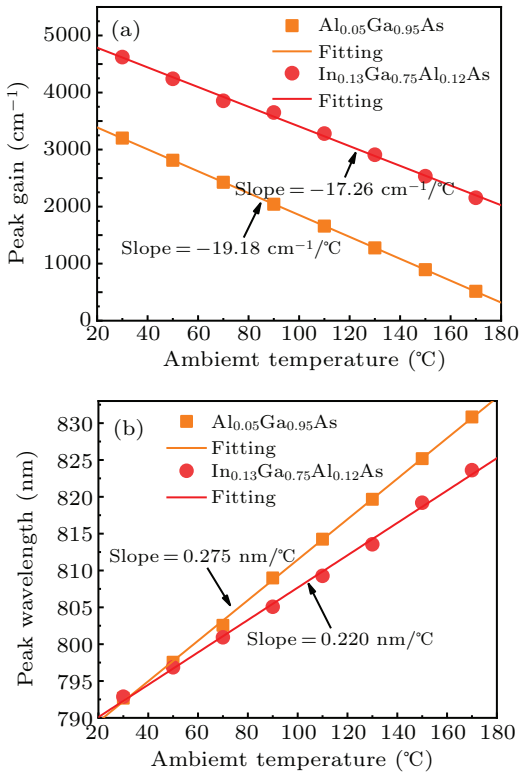


Fig. 3. Plots of (a) peak gain and (b) peak wavelength *versus* ambient temperature of $Al_{0.05}Ga_{0.95}As$ and $In_{0.13}Ga_{0.75}Al_{0.12}As$ quantum wells with 6-nm width.

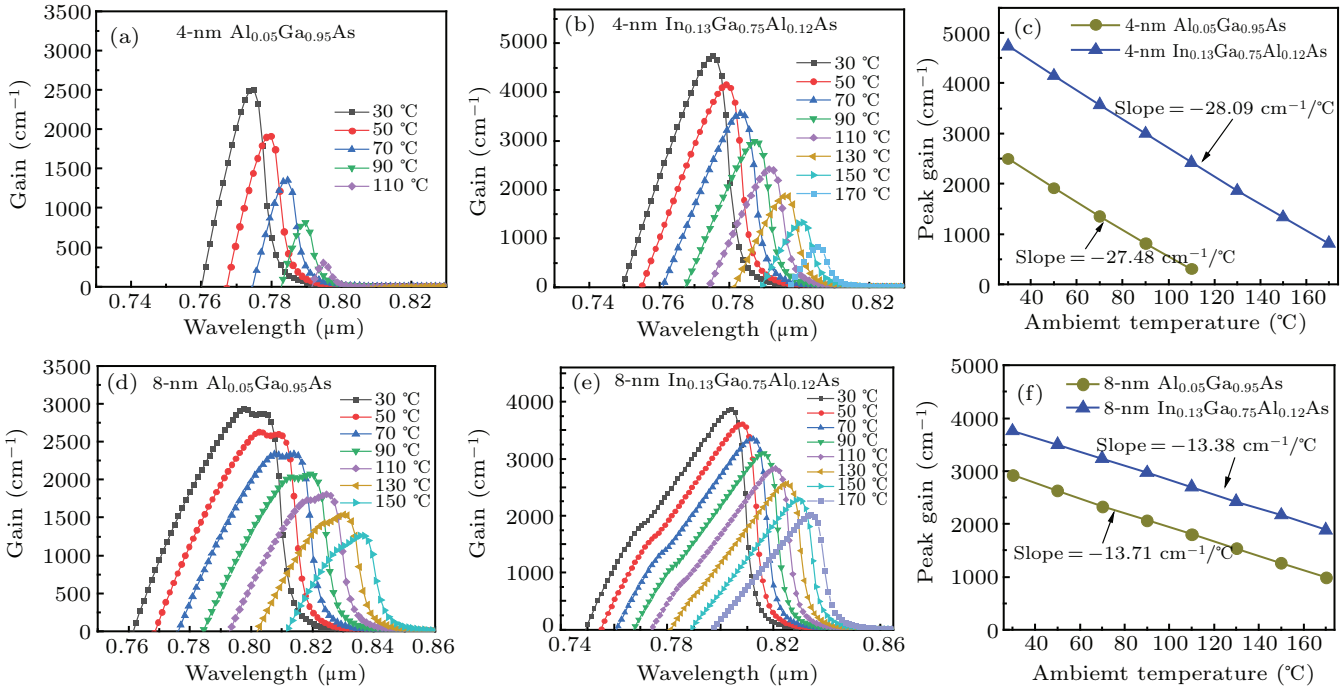


Fig. 4. Plots of gain *versus* wavelength of $Al_{0.05}Ga_{0.95}As$ quantum wells with (a) 4-nm and (d) 8-nm widths at different temperatures. Plots of gain *versus* wavelength of $In_{0.13}Ga_{0.75}$ $Al_{0.12}As$ quantum wells with (b) 4-nm and (d) 8-nm widths. Plots of peak gain *versus* ambient temperature of $Al_{0.05}Ga_{0.95}As$ and $In_{0.13}Ga_{0.75}$ $Al_{0.12}As$ quantum wells with (c) 4-nm and (f) 8-nm widths.

When the quantum well width is 4 nm, the peak-gain-dropping rate with temperature increasing for $In_{0.13}Ga_{0.75}Al_{0.12}As$ quantum wells and $Al_{0.05}Ga_{0.95}As$ quantum wells are 28.09 $cm^{-1}/°C$ and 28.66 $cm^{-1}/°C$, respectively. When the quantum well width is 8 nm, the peak-gain-dropping rate of $In_{0.13}Ga_{0.75}Al_{0.12}As$ quantum wells and $Al_{0.05}Ga_{0.95}As$ quantum wells are 13.38 $cm^{-1}/°C$ and 13.71 $cm^{-1}/°C$, respectively. Therefore, the $In_{0.13}Ga_{0.75}Al_{0.12}As$ is surely more stable than $Al_{0.05}Ga_{0.95}As$ quantum wells with the temperature varying. It is also found that the quantum well with larger width exhibits more stable

temperature performance. However, the gain decreases as the quantum well width increases. Therefore, the 6-nm well width is very suitable in terms of both gain and temperature stabilities.

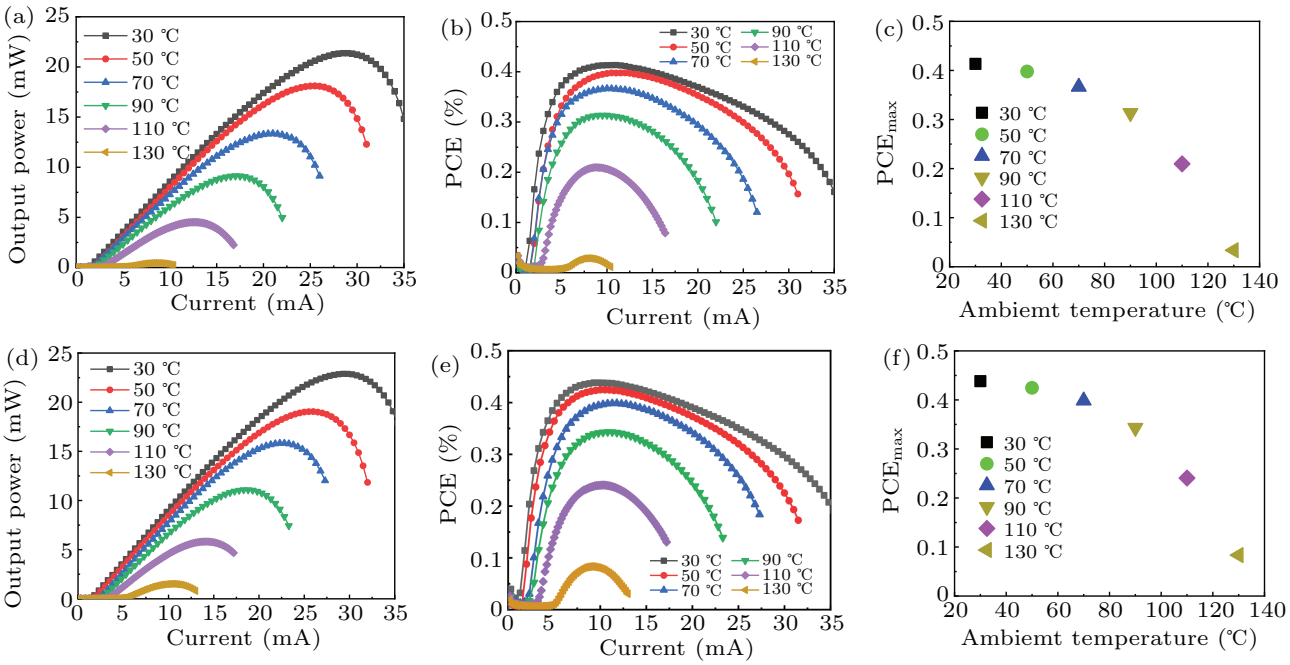


Fig. 5. Plots of (a) output power, (b) PCE, and (c) maximum PCE *versus* current of the $Al_{0.05}Ga_{0.95}As$ quantum wells VCSELs with 10-μm oxide aperture in a temperature range of 30 °C–130 °C, and plots of (d) output power, (e) PCE, and (f) maximum PCE *versus* ambient temperature of $In_{0.13}Ga_{0.75}Al_{0.12}As$ quantum wells VCSELs with 10-μm oxide aperture in a temperature range of 30 °C–130 °C.

The VCSELs with different oxide aperture diameters are fabricated and tested. The *L–I* characteristics of the 10-μm VCSELs with both $Al_{0.05}Ga_{0.95}As$ quantum wells and $In_{0.13}Ga_{0.75}Al_{0.12}As$ quantum wells at ambient temperatures ranging from 30 °C to 130 °C are shown in Figs. 5(a) and 5(b). It can be found that the output power of the $In_{0.13}Ga_{0.75}Al_{0.12}As$ quantum wells VCSELs is greater than that of the $Al_{0.05}Ga_{0.95}As$ quantum wells VCSELs at the same ambient temperature and injection current. The maximum output power of $In_{0.13}Ga_{0.75}Al_{0.12}As$ quantum wells VCSELs is 22.88 mW at 30 °C. As the ambient temperature increases, the output power gradually decreases. The maximum output power is 15.82 mW at 70 °C and 1.52 mW at 130 °C. The maximum power of $Al_{0.05}Ga_{0.95}As$ quantum wells VCSELs is 21.37 mW at 30 °C, 13.35 mW at 70 °C, and only 0.031 mW at 130 °C. The output power of $In_{0.13}Ga_{0.75}Al_{0.12}As$ quantum wells VCSELs decreases more slowly with the increase of ambient temperature. Therefore, the $In_{0.13}Ga_{0.75}Al_{0.12}As$ quantum wells VCSELs exhibit better high-temperature performances than $Al_{0.05}Ga_{0.95}As$ quantum wells VCSELs.

The power conversion efficiency (PCE) of the VCSELs with two kinds of quantum wells under different ambient temperatures are shown in Figs. 5(b) and 5(e). As the ambient temperature is 30 °C, the maximum power conversion efficiency (PCE) of $In_{0.13}Ga_{0.75}Al_{0.12}As$ quantum wells VCSELs can reach 43.82% which is higher than that of $Al_{.05}Ga_{0.95}As$ quantum wells VCSELs, 41.33%. As the ambient temperature increases to 130 °C, the maximum PCE for $In_{0.13}Ga_{0.75}Al_{0.12}As$ quantum wells VCSELs and $Al_{0.05}Ga_{0.95}As$ quantum wells VCSELs decrease to 8.35% and 3.36%, respectively. The plots of maximum PCE of the two devices *versus* ambient temperature are shown in Figs. 5(c) and 5(d). Obviously, the maximum PCE of the $Al_{.05}Ga_{0.95}As$ quantum wells VCSELs decreases faster with the increase of ambient temperature. Under the same operation condition, the $In_{0.13}Ga_{0.75}Al_{0.12}As$ quantum wells VCSELs have higher output power and higher power conversion efficiency than the $Al_{0.05}Ga_{.95}As$ quantum wells VCSELs, showing better high-temperature stability. The experimental results are consistent with the calculations.

Figure 6(a) shows the plots of peak output power *versus* ambient temperature of $In_{0.13}Ga_{0.75}Al_{0.12}As$ quantum wells VCSELs with six oxide aperture diameters in a range of 2 μm–25 μm. The peak output power of VCSELs with the same oxide aperture decreases almost linearly with ambient temperature increasing. The extracted drop rate of peak output power increasing with oxide aperture increasing is shown in Fig. 6(b). The drop rate of the peak output power of the VCSELs with an oxide aperture diameter of 2 μm, 10 μm, and 25 μm are 0.0471 mW/ °C, 0.1901 mW/ °C, and 0.4996 mW/ °C, respectively. This is because larger active region area produces more heat, which will introduce more serious heat crosstalk. The heat dissipation in large aperture VCSELs is more difficult than that in small aperture VCSELs. As the ambient temperature increases, the phenomenon turns more serious, which accelerates the temperature rise. Therefore, the small aperture VCSELs exhibit more stable temperature characteristics.

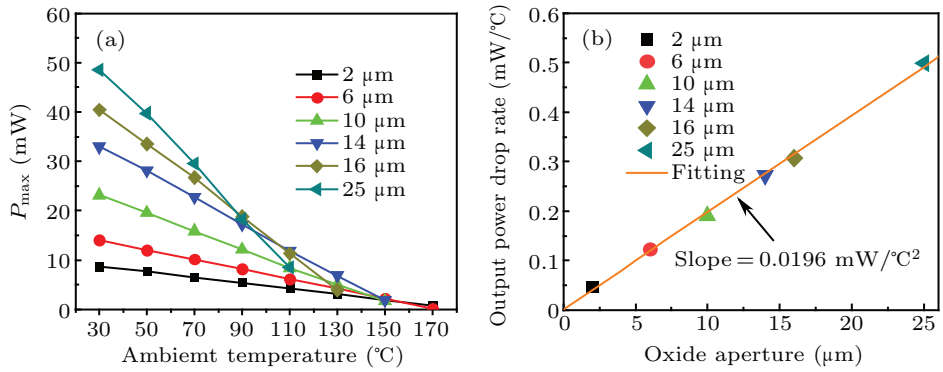


Fig. 6. (a) Plots of peak output power *versus* ambient temperature of $In_{0.13}Ga_{0.75}Al_{0.12}As$ quantum wells VCSELs with 2-μm–25-μm oxide apertures, and (b) plot of drop rate of peak output power *versus* oxide aperture.

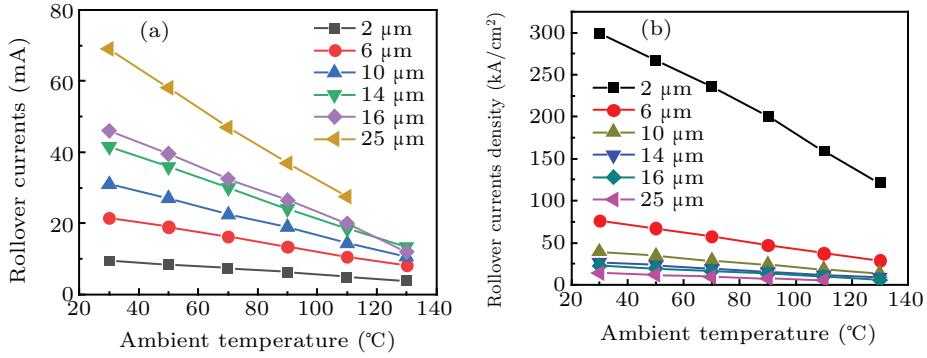


Fig. 7. (a) Rollover current and (b) rollover current density *versus* ambient temperature of 808-nm $In_{0.13}Ga_{0.75}Al_{0.12}As$ quantum wells VCSELs with 2-μm–25-μm oxide apertures.

The rollover current of VCSELs with an oxide aperture diameter of 2 μm and 25 μm at 30 °C are 9.4 mA and 69 mA, respectively. When the ambient temperature rises to 110 °C, the rollover currents become 5 mA and 27.5 mA, respectively, as shown in Fig. 7(a). It is noted that VCSELs with a larger oxide aperture have higher rollover currents. As the ambient temperature increases, the rollover current of the VCSELs with large oxide aperture decreases more quickly than that of the VCSELs with small oxide aperture. Figure 7(b) shows that the plots of rollover current density of VCSELs *versus* current density for different oxide apertures. The rollover current density of 2-μm and 25-μm VCSELs at 30 °C are 299.21 kA/cm^2 and 14.06 kA/cm^2, respectively. As the temperature increases to 110 °C, the rollover current density decreases to 159.15 kA/cm^2 and 5.60 kA/cm^2, respectively. It indicates that the rollover current density of VCSELs with larger oxide aperture is smaller. With the increase of ambient temperature, the rollover current density of the VCSELs with small oxide aperture decreases faster than that of the VCSELs with large oxide aperture.

The plots of the output power of the $In_{0.13}Ga_{0.75}Al_{0.12}As$ quantum wells VCSELs *versus* injection current are shown in Fig. 8(a). The changes of output power of VCSELs with different oxide apertures are basically the same under small injection currents. As the injection current increases, the output power of the VCSELs with small oxide aperture decreases faster because the VCSELs with small oxide aperture has a small rollover current. Figure 8(b) shows the change of the output power of the $In_{0.13}Ga_{0.75}Al_{0.12}As$ quantum wells VCSELs with injection current density as the ambient temperature increases from 30 °C to 90 °C. Under the same current density, the change of output power increases with the augment of the oxide aperture diameter. This is because the rollover current density of VCSELs with large oxide aperture is lower than that of VCSELs with small oxide aperture. Obviously, the VCSELs with small oxide aperture have more excellent high-temperature stability than large oxide aperture VCSELs.

To investigate the thermal characteristics of $In_{0.13}Ga_{0.75}Al_{0.12}As$ quantum wells VCSELs, the thermal resistance is also calculated according to the emission spectra and the dissipated power. Thermal resistance can be determined experimentally from the following equation:[25]

$$R_{\rm th} = \frac{\Delta T}{\Delta P_{\rm diss}} = \frac{\Delta\lambda/\Delta P_{\rm diss}}{\Delta\lambda/\Delta T_{\rm hs}}, \tag{1}$$

where $\Delta\lambda/\Delta P_{\rm diss}$ is calculated by the variation of the wavelength shift with the dissipated power. The dissipation power is calculated by the input power subtracting the output power. Figure 9(a) shows that the value of $\Delta\lambda/\Delta P_{\rm diss}$ of $In_{0.13}Ga_{0.75}Al_{0.12}As$ quantum wells VCSELs with 10-μm oxide aperture at 30 °C, 50 °C, 70 °C, 90 °C, and 110 °C are 0.1325 nm/mW, 0.1366 nm/mW, 0.1434 nm/mW, 0.1525 nm/mW, and 0.1615 nm/mW, respectively. $\Delta\lambda/\Delta T_{\rm hs}$

is calculated by the peak wavelength shift rate *versus* ambient temperature, and its value is 0.0602 nm/°. At the ambient temperatures of 30 °C, 50 °C, 70 °C, 90 °C, and 110 °C, the thermal resistances are 2.201 K/mW, 2.269 K/mW, 2.382 K/mW, 2.533 K/mW, and 2.683 K/mW, respectively, as shown in Fig. 9(b).

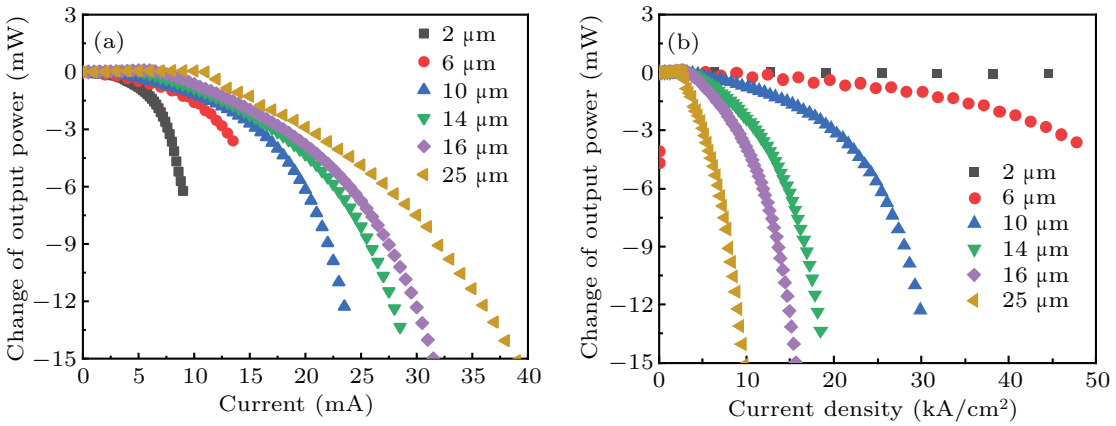


Fig. 8. Plots of output power of $In_{0.13}Ga_{0.75}Al_{0.12}As$ quantum wells VCSELs *versus* (a) injection current and (b) injection current density as ambient temperature increases from 30 °C to 90 °C.

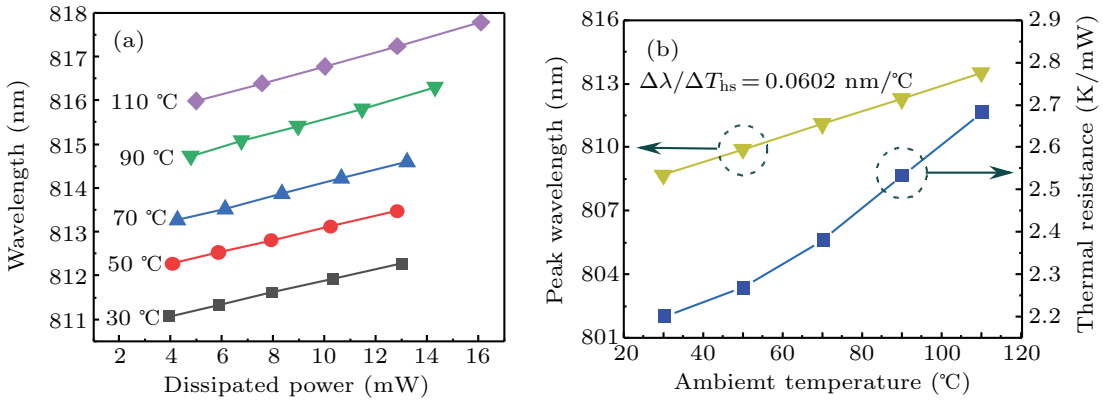


Fig. 9. (a) The $\Delta\lambda/\Delta P_{diss}$ of $In_{0.13}Ga_{0.75}Al_{0.12}As$ quantum wells VCSELs with 10-μm oxide aperture *versus* dissipated power at different ambient temperatures, and (b) $\Delta\lambda/\Delta T_{hs}$ and thermal resistance *versus* ambient temperature.

4. Conclusions

In conclusion, the theoretical calculations show that the strained $In_{0.13}Ga_{0.75}Al_{0.12}As/Al_{0.3}Ga_{0.7}As$ quantum wells possess higher material gain and lower temperature sensitivity than the $Al_{0.05}Ga_{0.95}As/Al_{0.3}Ga_{0.7}As$ quantum wells. The 808-nm vertical cavity surface emitting lasers with various oxide apertures are fabricated and characterized in this paper. It is demonstrated that the vertical cavity surface emitting lasers with strained $In_{0.13}Ga_{0.75}Al_{0.12}As/Al_{0.3}Ga_{0.7}As$ quantum wells exhibit higher power conversion efficiency (PCE) and better temperature stability. Such the vertical cavity surface emitting laser of 808-nm $In_{0.13}Ga_{0.75}Al_{0.12}As/Al_{0.3}Ga_{0.7}As$ quantum wells will be preferred for high power applications. The maximum PCE of 43.8% for 10-μm VCSELs is achieved at the ambient temperature of 30 °C. The output power and spectra of the VCSELs under different ambient temperatures are tested. We find that the smaller oxide aperture VCSELs exhibit more stable temperature performance. The thermal resistances at different temperatures are also presented.

Acknowledgements

Project supported by the National Natural Science Foundation of China (Grant No. 61804175), the Key Research Program of Frontier Sciences, Chinese Academy of Sciences (Grant No. ZDBS-LY-JSC031), and the China Postdoctoral Science Foundation (Grant No. BX20200358).

References

[1] Huffaker D L and Deppe D G 1994 *Appl. Phys. Lett.* **65** 97
[2] Valle A, Sciamanna M and Panajotov K 2007 *Phys. Rev. E* **76** 046206
[3] Jaeger R, Grabherr M, Jung C, Michalzik R, Reiner G, Weigl B and Ebeling K J 1997 *Electron. Lett.* **33** 330
[4] Larisch G, Moser P, Lott J A and Bimberg D 2016 *IEEE Photon. Technol. Lett.* **28** 2327
[5] Xun M, Pan G Z, Zhao Z Z, Sun Y, Zhou J T and Wu D X 2021 *IEEE Trans. Electron. Dev.* **68** 2829
[6] Xiang L, Zhang X, Zhang J W, Huang Y W, Ning Y Q and Wang L J 2017 *Chin. Phys. B* **26** 074209
[7] Seurin J F, Ghosh C L, Khalfin V, Miglo A, Xu G, Wynn J D, Pradhan P and D'Asaro L A 2008 *Proc. SPIE* **6908** 690808
[8] Seurin J F, Zhou D, Xu G, Miglo A and Ghosh C 2016 *Proc. SPIE* **9766** 97660
[9] E. Hugues-Salas, Giddings R P, Jin X Q, Wei J L, Zheng X, Hong Y, Shu C and Tang J M 2011 *Opt. Express* **19** 2979

[10] Harris J S, Sullivan T O, Sarmiento T, Lee M M and Vo S 2010 *Semicond. Sci. Technol.* **26** 14010

[11] Xun M, Sun Y, Xu C, Xie Y Y, Jin Z, Zhou J T, Liu X Y and Wu D X 2018 *Chin. Phys. Lett.* **35** 034202

[12] Hariyama T, Sandborn P A M, Watanabe M and Wu M C 2018 *Opt. Express* **26** 9285

[13] Wang L J, Ning Y Q, Zhang X, Zhong C Y, Werner and Hofmann 2018 *IEEE Photon. J.* **10** 1

[14] Di P C, Li X P, Yang J, Wang R J and Peng Q J 2021 *IEEE Photon. Technol. Lett.* **33** 395

[15] Hao Y Q, Ma J L and Yan C L 2013 *Laser Phys. Lett.* **10** 055003

[16] Hession M T, Markova A and Graber E M 2015 *Dermatol. Surg.* **41** 307

[17] Geske J, Wang C, MacDougal M, Stahl R, Follman D, Garrett H, Meyrath T, Snyder D, Golden E, Wagener J and Foley J 2010 *Proc. SPIE* **7615** 76150

[18] Seurin J F, Xu G, Guo B, Miglo A, Wang Q, Pradhan P, Wynn J D, Khalfin V, Zou W X, Ghosh C L and Leeuwen R V 2011 *Proc. SPIE* **7952** 669

[19] Seurin J F, Xu G, Khalfin V, Miglo A, Wynn J D, Pradhan P, Ghosh C L and D'Asaro L A 2009 *Proc. SPIE* **7229** 722903

[20] Zhong C Y, Zhang X, Hofmann W, Ning Y Q and Wang L J 2018 *IEEE Photon. J.* **10** 1504608

[21] Zhang Y, Ning Y Q, Zhang L, Zhang J S, Zhang J W, Wang Z F, Jian Z, Zeng Y G and Wang L J 2011 *Opt. Express* **19** 12569

[22] Fujisawa T, Sato T, Mitsuhara M, Kakitsuka T, Yamanaka T, Kondo Y and Kano F 2009 *IEEE J. Quantum Electron.* **45** 1183

[23] Zhao Z Z, Xun M, Pan G Z, Sun Y, Zhou J T, Wang D H and Wu D X 2021 *Acta Phys. Sin.* **70** 114202 (in Chinese)

[24] Coldren and Larry A 1995 *Opt. Eng.* **36** 616

[25] Xun M, Pan G Z, Zhao Z Z, Sun Y, Yang C Y, Kan Q, Zhou J T and Wu D X 2020 *IEEE Trans. Electron. Dev.* **68** 158